Fourier Transform Based Hyperspectral Imaging

Marco Q. Pisani and Massimo E. Zucco
National Institute of Metrological Research
Italy

1. Introduction

A hyperspectral imaging system (HSIS) is a combination of an imaging device and a spectrometer. The result is a 2D image combined with the third dimension containing the spectral composition of each pixel of the image. Spectrometers normally implemented in hyperspectral imaging systems are made by integrating a dispersive means (a prism or a grating) in an optical system, with the drawback of having the image analyzed per lines and some mechanics integrated in the optical system, cfr. Fig 1, (Sellar & Boreman, 2005).
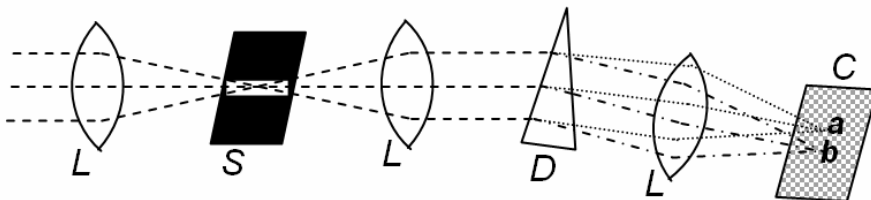

Fig. 1. Classical "pushbroom" hyperspectral imaging camera. L: collimating lenses, S: entrance slit selecting a row of the image in the focal plane; D: dispersive means (prism or grating) dispersing light in the direction orthogonal to the entrance slit; C: camera sensor where the combined image is focused. Points *a* and *b,* representing a pixel of the row selected at the entrance, are imaged at different vertical coordinates

Alternatively, HSIS devices are based on optical band-pass filters either tuneable or fixed and the spectrum has to be scanned in steps. In Fig 2 an example of the spectral transmissivity of a tunable band pass filter. Since the spectral transmissivity depends on the wavelength, HSIS systems have to be calibrated in advance and some mathematical manipulations are required to obtain the final hyperspectral image.

A third kind of spectrometer implemented in HSIS is based on interferometers (Alcock & Coupland, 2006), where the spectrum for each pixel is obtained by applying Fourier transform based algorithm to the signal (called interferogram) obtained by scanning the optical path difference *OPD*. The same technique has been used for decades by spectroscopists to obtain high resolution absorption spectra by using Michelson (or two-beam) or Fabry-Perot F-P (multi-beam) interferometer. There are many features that make

interferometer based spectrometers superior to conventional spectrometers. First, the Felgett or multiplex advantage arises from the fact that there is no spectral scanning and all the spectral components are acquired at the same time. Second, the Jacquinot or throughput advantage originates from the fact that the aperture used in FTIR spectrometers has a larger area than the slits used in dispersive spectrometers, thus enabling higher throughput of radiation. These two effects combined together make the interferometer based spectrometer a faster (or equivalently having a higher luminosity) instrument with respect to the other spectrometers at the same resolution. We have realized a HSIS based on a F-P spectrometer that will be discussed in details in section 3. In section 4 the application of our HSIS will be presented. In section 2 the mathematical manipulation to obtain spectra with the Michelson spectrometer will be discussed.
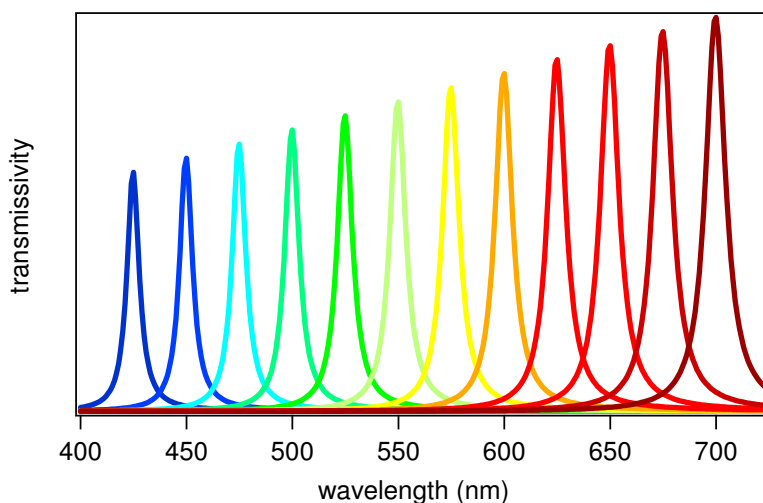

Fig. 2. The spectral response of a tunable filter to be used for HSIS

2. Michelson spectrometer

This section is devoted to the presentation of the Michelson spectrometer and to the mathematical manipulation to calculate spectra. In a Michelson spectrometer (Fig 3) the incoming light is divided in two beams by the beam splitter, after the two beams have travelled different paths, they are finally recombined on the detector where interference is measured. The intensity on the detector varies with the optical path difference *OPD* or retardation δ, double of the mirror displacement *x*.

When the incoming light is emitted by a monochromatic source and the two beams have the same intensity on the detector, the interferogram signal is represented by the equation

$$\overline{I}\left(\delta\right)=0.5B\left(\tilde{v}_o\right)\left(1+\cos\left(2\pi\tilde{v}_o\delta\right)\right) \tag{1}$$

where $\tilde{v}_o$ is the wavenumber $\tilde{v}_o=1/\lambda_o$ and $B\left(\tilde{v}_o\right)$ represents the intensity of the source at $\tilde{v}_o$. By using the frequency $v_o=c\tilde{v}_o=c/\lambda_o$, equation (1) is transformed in:

$$\overline{I}(\delta) = 0.5B(\nu_o)\big(1 + \cos(2\pi\nu_o\,\delta/c)\big) \tag{2}$$

The interferogram in (2) has two components, a constant component equal to $0.5B(\tilde{\nu}_o)$ and a modulated component equal to

$$\overline{I}(\delta) = 0.5B(\nu_o)\cos(2\pi\nu_o\,\delta/c) \tag{3}$$

Equation (3) is incomplete, there are several factors that reduce the spectral response of the system and the resulting signal: the optical elements (beam splitter, mirrors, lenses) and detectors normally have a non uniform responsivity. Moreover, the electronic devices used to condition the signal have a non uniform frequency dependence. All these different contributions are counted in the term $S(\nu_o)$, giving

$$\overline{I}(\delta) = S(\nu_o)\cos(2\pi\nu_o\,\delta/c) \tag{4}$$

When the source is broadband and continuum, the interferogram can be represented by the cosine Fourier Transform integral

$$I(\delta) = \frac{1}{c}\int\limits_{-\infty}^{\infty} S(\nu)\cos(2\pi\nu\,\delta/c)d\nu \tag{5}$$

and the spectrum by

$$S(\nu) = 2\int\limits_{0}^{\infty} I(\delta)\cos(2\pi\nu\,\delta/c)d\delta \tag{6}$$

I(δ) in (6) is based on an infinite and continuum retardation δ. In practice, the signal is sampled at finite sampling interval Δs and consists of N discrete, equidistant points and equation (6) transforms in (7), where all the constants have been discarded: the discrete version of the cosine FT, discrete cosine transform DCT. The maximum retardation is N Δs.

$$S[k\cdot\Delta\nu] = \sum_{n=0}^{N-1} I[n\cdot\Delta s]\cos(2\pi nk/N) \tag{7}$$

DCT means that in the time domain the Fourier series decomposes the periodic function into a sum of cosine and in the frequency domain it could be seen as if the signal intensity is divided in multiple adjacent frequency bins. For N equi-spaced points in the retardation at interval N Δs, we have N equi-spaced bins in the spectrum with spacing $\Delta\nu$ related to Δs by the formula

$$\Delta\nu = \frac{c}{N\Delta s} = \frac{c}{\delta_{max}} \tag{8}$$

Therefore the resolution $\Delta\nu$ is inversely proportional to total retardation δ_{max}. Considering the total mirror displacement L from zero retardation, the resolution will be $\Delta\nu = \dfrac{c}{2L}$. As an example, for L = 20 μm, we obtain $\Delta\nu$ = 7.5 THz.
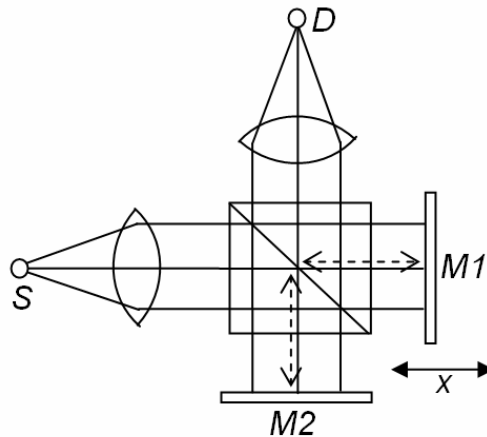
Fig. 3. Set-up of the Michelson spectrometer. S is the light source, D is the detector, M1 and M2 are two plane mirrors (or corner cube retro-reflectors). M1 moves back and forth unbalancing the optical path difference (*OPD*) of the interferometer

A laser at 633 nm is normally incorporated in Michelson spectrometers to calibrate the mirror displacement and to acquire the retardation at equal intervals of retardation. There are two ways to perform the interferogram acquisition synchronized with the mirror displacement, one is by moving the mirror at constant velocity in the retardation, this means that for a mirror velocity of 1 cm/s the acquired signal is at tens of kHz. The other method is by equispaced steps, for each single step one point of the interferogram is acquired.

As will be seen in Fig 6 in the next section, DCT generates a spectrum formed by the fundamental spectrum plus its mirror image, only the first N/2 points of equation (7) are useful, the second set of N/2 are redundant and discarded. A spectrum is meaningful if there is no overlap between the fundamental spectrum and the symmetrical replicas, therefore if the fundamental spectrum is completely contained in the first N/2 bins and is zero in the remaining N/2 bins. This is called Nyquist criterion, in order to sample a signal the sampling device should include a low pass filter that cuts the frequencies higher than half the sampling rate.

DCT in (7) is based on symmetrical interferograms around the zero retardation. When optics is dispersive and/or conditioning electronics have a phase dependence on frequency the interferogram becomes asymmetrical and DCT cannot be used directly. There are some techniques (Griffiths & de Haseth, 2007) to calculate the phase correction from the complex DFT.

The instrumental lineshape ILS function represents the resolution of the spectrometer and corresponds to the spectrum measured by the spectrometer when the radiation is monochromatic. ILS is the filter shape of each frequency bin. When the interferogram acquisition is abruptly truncated at the extremes, the rectangular or boxcar cutoff creates an ILS having the shape of a "sinc" function centered on the frequency bin, having a narrow peak but with important sidelobes that would hide possible neighbor lines. There is a palette of ILS function available to trade between the resolution (related to the width of the peak) and to the amplitude accuracy (related to the amplitude of the tails). ILS function can

varied by multiplying the acquired interferogram by an appropriate tapering function (Smith, 1999), (Weisstein).

As was described before, the frequency bin interval is inversely proportional to the total retardation. If a monochromatic component has a period that is not exactly a submultiple of the total retardation, the frequency falls between adjacent bins and spectral components would be spread in several adjacent bins. Adding a series of zeros at the end of the interferogram has the important effect that new bins are created and the spectrum is interpolated in correspondence of the new bins and more frequencies could be represented without being spread.

Apparently, as stated in eq (8) the resolution $\Delta\nu$ is only limited by the maximum retardation of the interferometer and therefore by increasing the retardation there is no physical limit to the attainable resolution. In practice the detector has a finite dimension and the considered rays pass through the interferometer with a divergence half-angle a. For a certain frequency νo and divergence a, it is always possible to find a retardation δ_{max} such that the rays interfere destructively on the detector. This retardation δ_{max} inserted in eq. (8) limits the minimum attainable resolution and there is no advantage to use a retardation longer than δ_{max}. The formula that relates the divergence half-angle a to the resolution $\Delta\nu$ is the following:

$$\Delta\nu = \alpha^2\, \nu_o \tag{9}$$

3. F-P spectrometer

After having considered how it is possible to calculate a spectrum with the Michelson spectrometer by using the mathematical manipulations based on DCT, we now describe F-P spectrometers, core of the HSIS we have developed, and the associated algorithm to calculate the spectrum (Pisani & Zucco, 2009).
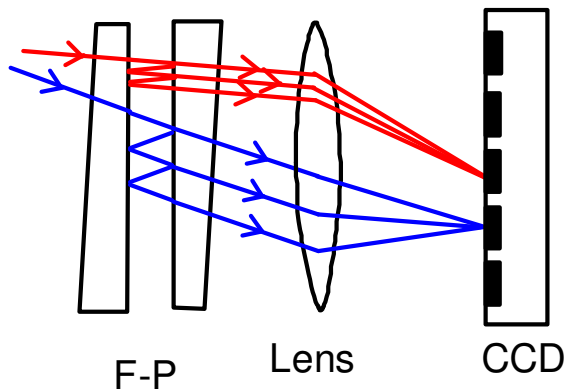

Fig. 4. Scheme of the F-P interferometer

The F-P spectrometer set-up is presented in Fig 4, and it is formed by two semireflective mirrors having reflectivity R at a distance d. For simplicity we consider mirrors with metallic

coating with the peculiarity of having a negligible dispersion in the visible and in the IR region or equivalently a constant penetration depth versus the frequency. The incoming beam is reflected many times by the reflective surfaces and the different refracted beams are finally combined on the detector. The resulting interferogram for a monochromatic source at frequency v_o is the Airy function

$$\overline{I}(\delta) = S(v)\frac{1}{1+\left(\dfrac{4R}{(1-R)^2}\right)\sin^2(2\pi vd/c)} \tag{10}$$

Comparing the F-P interferogram (10) with the Michelson interferogram in (4) for a monochromatic source, it is evident that the interferogram is formed by fringes having the same periodicity, but with fringes more pronounced at the increasing of R, as in Fig 5.
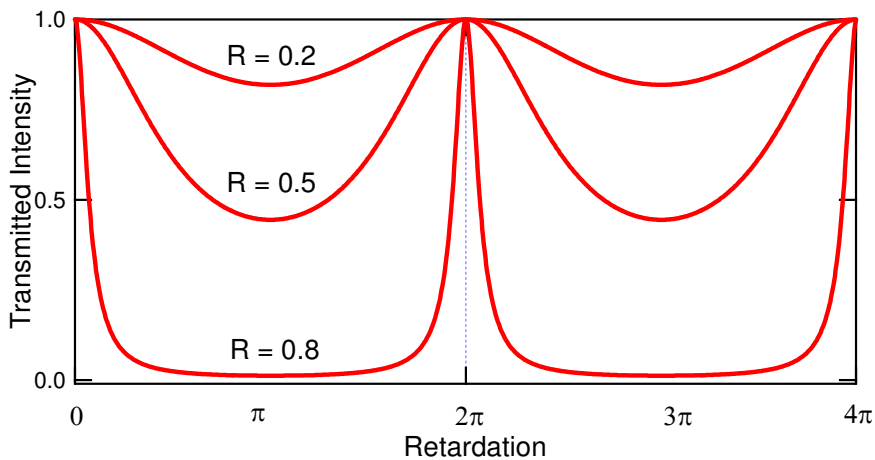
Fig. 5. Interferogram from the F-P spectrometer for different R

When the source is broadband and continuum, the resulting interferogram can be obtained by the integration of the different monochromatic contributions giving:

$$I(\delta) = \int_{-\infty}^{\infty} S(v)\frac{1}{1+\left(\dfrac{4R}{(1-R)^2}\right)\sin^2(2\pi vd/c)}dv \tag{11}$$

In the approximation that the reflectivity R of the mirrors is very low $R<<1$, the Airy fringes in (10) could be approximated with cosine function and eq (10) becomes

$$\overline{I}(\delta) = S(v)\frac{1}{1+\left(\dfrac{4R}{(1-R)^2}\right)\sin^2(2\pi vd/c)} \approx S(v)(1-2R) + S(v)2R\cos(\pi vd/c) \tag{12}$$

Taking into account only the modulated part of the interferogram (12), and including all the responsivity contributions in intensity of the radiation at the detector in $S(v_o)$, we obtain a equation similar to (3) and therefore the interferogram from the F-P could be solved using the DCT as in (6), provided that Nyquist criterion is respected, i.e. at least two points per fringe are acquired.
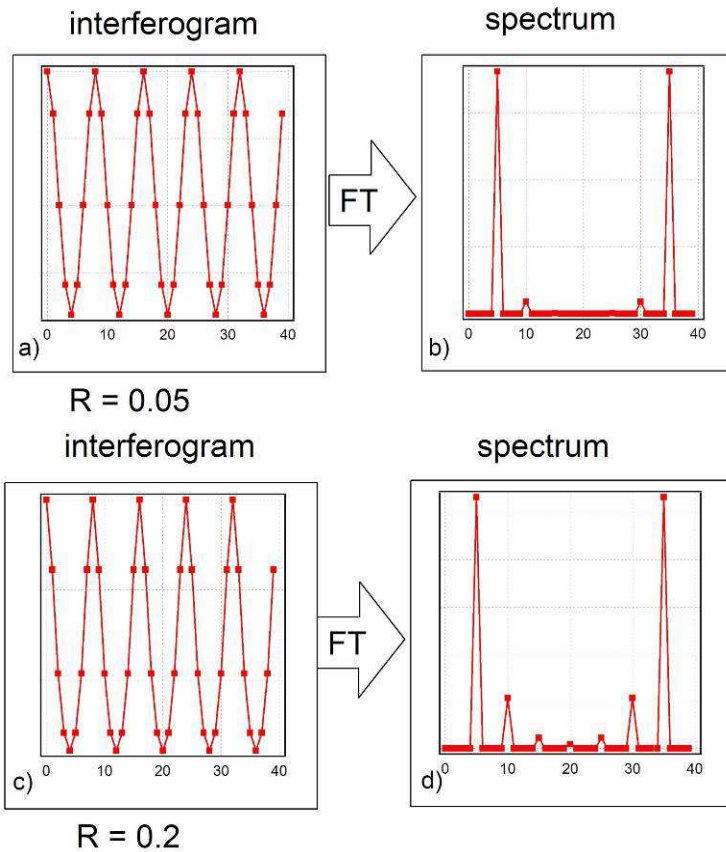

Fig. 6. Spectra obtained with DCT from F-P interferogram with different reflectivity. a) and b) interferogram and spectrum for reflectivity R = 0.05. c) and d) interferogram and spectrum for reflectivity R = 0.2

When the approximation presented in (12) is not possible because R is close to 1, we could still apply DCT to the Airy fringes, since the interferogram is periodic and can be decomposed by the Fourier series into a sum of cosines. Since the Airy fringes are far from being a cosine, also the higher harmonic components are presents. As an example in Fig 6. we have represented a F-P interferogram of a monochromatic source when R = 0.05, cfr. Fig 6(a), the associated DCT is presented in Fig 6(b) and the second harmonic is about $1/20$th of the fundamental whereas the third harmonic is negligible. In this example, the fringe is well oversampled, 8 points per fringe are acquired and Nyquist criterion is respected since it is

possible to see that the harmonics fade away in the higher part of the spectrum, and the aliases do not "superpose" with the fundamental spectrum. On the contrary, in a situation similar to the practical case that we will describe in the next section, when $R = 0.2$ the Airy fringes are more pronounced and by applying the DCT we see in Fig 6(d) that the 3rd and 4th harmonics are present and the 7th harmonic of the alias would sum up with the fundamental. Since the 6th harmonic is about $3 \cdot 10^{-5}$ of the fundamental, we state that is effect is negligible and by acquiring 8 points per fringe for $R = 0.2$ is enough to respect Nyquist criterion.

If now we consider a source with a broad spectrum larger than an octave in the electromagnetic spectrum, the second harmonic of the low frequency side would sum up with the fundamental spectrum in the high frequency side as is depicted in Fig 7(a). In this figure the fundamental spectrum is represented in red and is larger than an octave, the second harmonic in blue is superposed with the high frequency side of the spectrum. The sum of all the harmonics would give the resulting spectrum in black, and from its analysis is nearly impossible to obtain information about the fundamental spectrum in red. When the fundamental spectrum is smaller than an octave, as in Fig 7(b), from the resulting spectrum it is possible to discriminate from the fundamental and the second harmonic spectra.
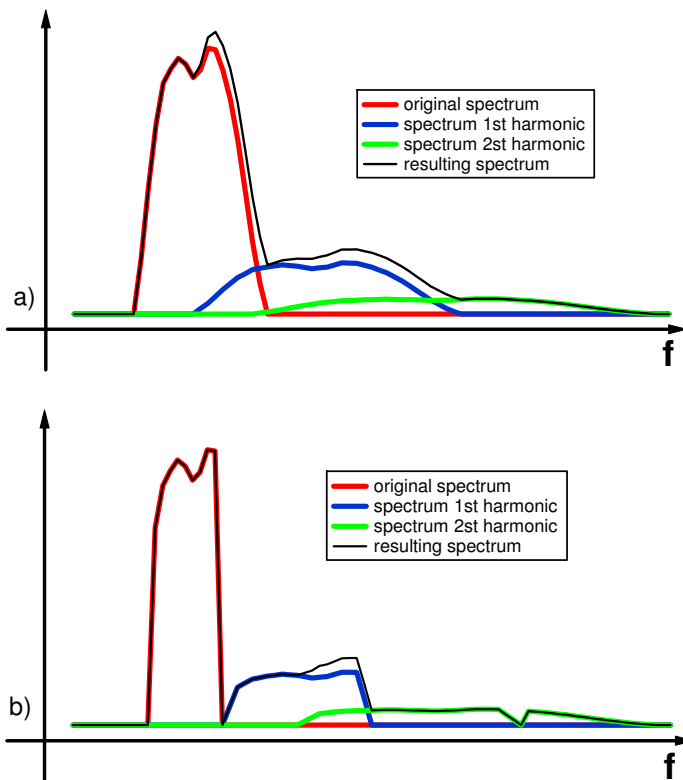

Fig. 7. Effect of superposition between harmonics of the fundamental spectrum. a) the spectrum is larger than an octave and it is not possible to discriminate from the fundamental and second harmonic b) the spectrum is smaller than an octave

While Michelson spectrometers have a double sided interferogram and this fact is useful in order to obtain information about the phase correction, the F-P interferogram is evidently single-sided and it does not start from the central or zero fringe when the mirrors come in contact because of the penetration depth of the radiation in the metallic coating. The latter implies that the interferogram is incomplete (i.e. it does not contain the data corresponding to the zero retardation condition), therefore it is not possible to apply directly the DCT to the interferogram as in two beam interferometers. As an example, in Fig 8 is presented the measured interferogram obtained from a F-P having a metallic coating of a laser radiation at $\lambda = 410$ nm. It is possible to see that the first half of the fringe is missing, corresponding to a retardation of 205 nm or equivalently to a mirror distance of 102.5 nm, we can estimate that the penetration depth of the metallic layer is smaller than 50 nm.
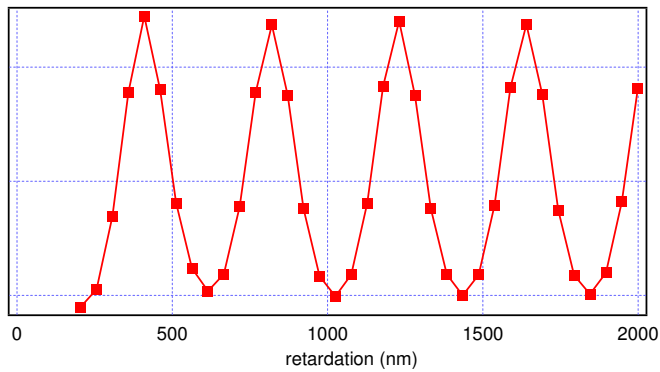
Fig. 8. The measured interferogram of a laser radiation at $\lambda = 410$ nm. The estimated penetration depth of the metallic layer is smaller than 50 nm
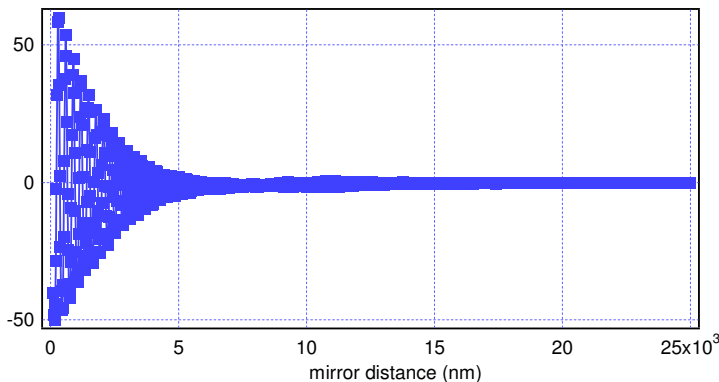

Fig. 9(a). The interferogram of a yellow LED with a maximum mirror distance $\delta = 25$ µm

The two aforementioned problems (presence of harmonics and missing points) are solved in our prototype by introducing an optical bandpass filter in the optical system transmitting slightly less than one octave of the electromagnetic spectrum, as the spectrum reported in Fig 7(b). This solution reduces the region of measurable spectrum but has the important

consequence that by using the information that certain region of the spectrum have zero intensity it is possible to estimate the value of the missing points in the interferogram and reconstruct the spectrum. As an example, consider the interferogram in Fig 9 of a yellow LED with a maximum mirror scan distance of δ = 25 μm corresponding to a resolution of about 6 THz, according to equation (8). To calibrate the mirror distance a blue laser at 410 nm is used and the points are acquired at interval of 25.5 nm in mirror distance. In Fig 9(a) it is presented the plot of the acquired interferogram. Due to the penetration depth, the first four points are missing. In Fig 9(b) the zoom of Fig 9(a) near the contact zone, zero retardation.
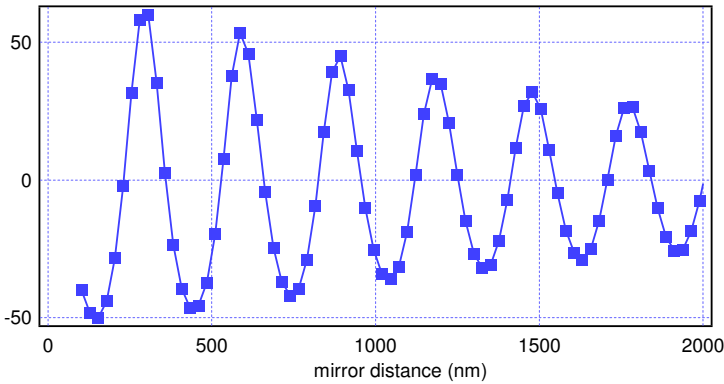
Fig. 9(b). The zoom of the interferogram in Fig 9(a) with the 4 missing points

Since the interferogram of Fig 9 is incomplete, four points are missing, it cannot be elaborated by the DCT in eq (7). In order to apply DCT the interferogram is completed with four points set at zero, not having any information *a priori*, and the result is presented in Fig 10.
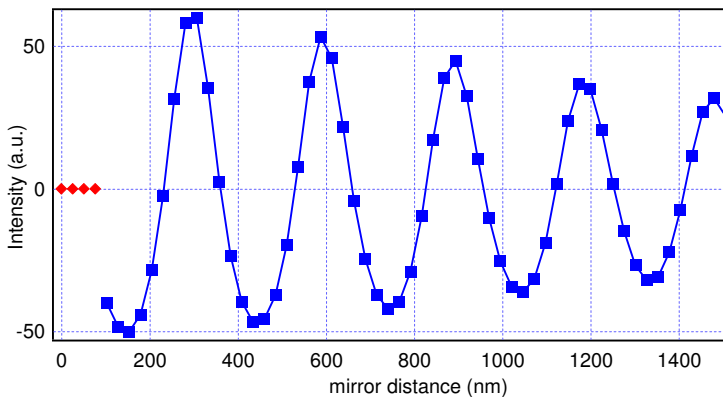

Fig. 10. The interferogram in Fig 9 with the 4 missing points (red diamonds) set at zero

The DCT of the interferogram gives the spectrum presented in Fig 11 where it is visible the spectrum of the yellow LED at about 500 THz and the second harmonic at about 1000 THz.

The spectra are sitting on a curved background due to the 4 missing points. In fact, according to the DCT equation where each point in the interferogram corresponds to a cosine contribution in the spectrum: the first missing point corresponds to the DC level in the spectrum, the second missing point corresponds to the cosine component having a period equal to the full spectrum span, and so on.
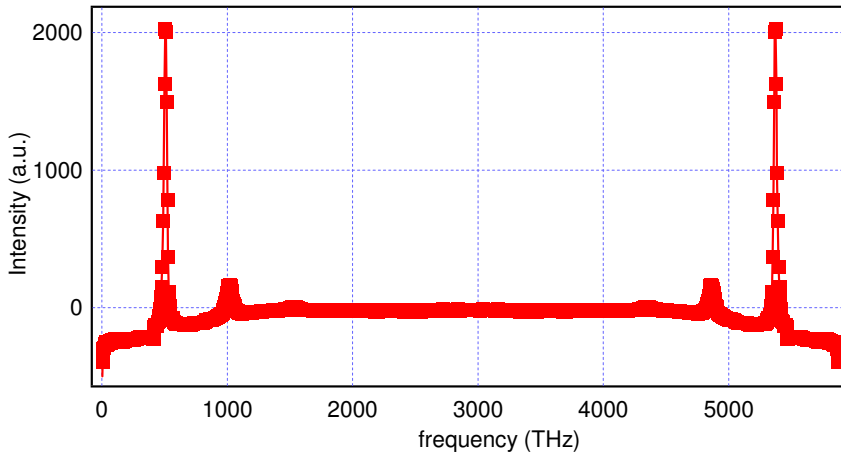

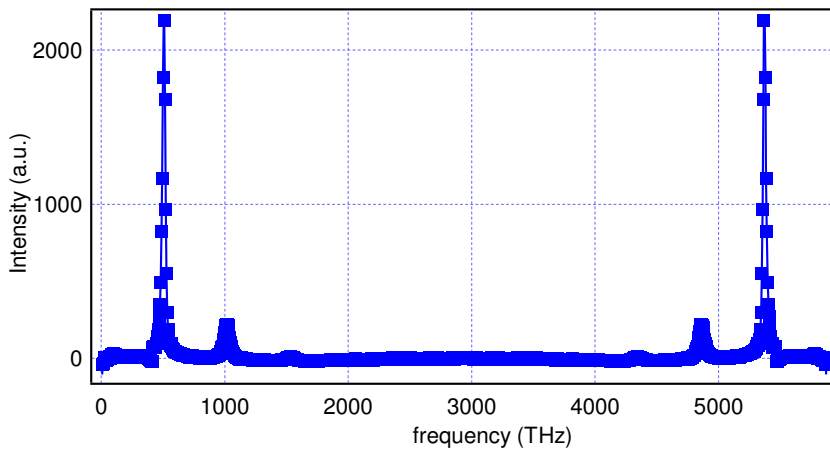Fig. 11. The "biased" spectrum obtained by applying the DCT to the incomplete interferogram in Fig 10

Fig. 12. The spectrum versus frequency of the yellow LED obtained by reconstructing the four missing points

By using the information that the spectrum has to be zero in certain region (the optical filters stops optical frequencies lower than 380 THz and higher than 720 THz), it is possible to find the amplitude of the four missing cosines and the value of the four missing points. In Fig 12 the reconstructed spectrum of the yellow LED with the fundamental spectrum at about 500

THz, the second harmonic at about 1000 THz and the third harmonic is nearly visible. In Fig 13 the spectrum in the pass band region of the optical filter represented in wavelength. In Fig 14 the interferogram with the reconstructed four missing points.
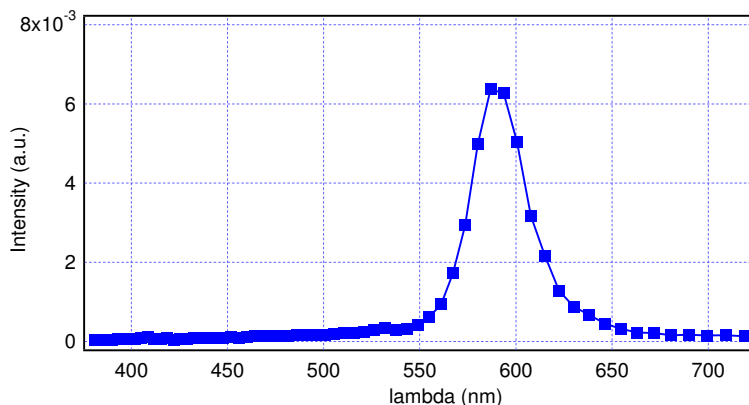

Fig. 13. The spectrum versus wavelength of the yellow LED in Fig 12
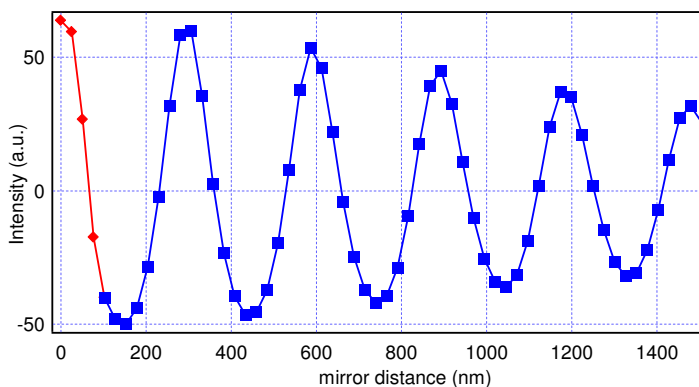

Fig. 14. Corrected interferogram to obtain the spectrum in Fig 12 and Fig 13. Blue squares: the original incomplete interferogram, red diamonds the reconstructed four points

In this section we have described the mathematical manipulations to calculate the spectrum from the incomplete F-P interferogram, in the next section we will explain how the F-P spectrometer could be integrated in an imaging system and obtain a HSIS.

4. Hyperspectral imaging prototype

In this section we describe how the F-P spectrometer is integrated in the HSIS, how the acquisition system is done and some applications in spectroscopy, colorimetry and thermal imaging.

The core of the device is the scanning F-P spectrometer described in section 3 and whose rendering is presented in Fig 15. The two mirrors are coated with a thin aluminum layer and

have a reflectivity of about 20%. The dispersion of the metallic coating has been demonstrated to be negligible for our applications in the spectral interval (0.4 – 1.7 um). The mirrors are mounted in aluminum frames and the distance is scanned by means of three piezo actuators allowing a maximum displacement of 60 µm at 100 V. A system made by three elastic hinges and three screws allows the optimal alignment and working distance of the mirrors to be found, so that, when the actuators are completely retracted (maximum voltage applied), the mirrors are in contact and the contact area is sufficiently large and centered.
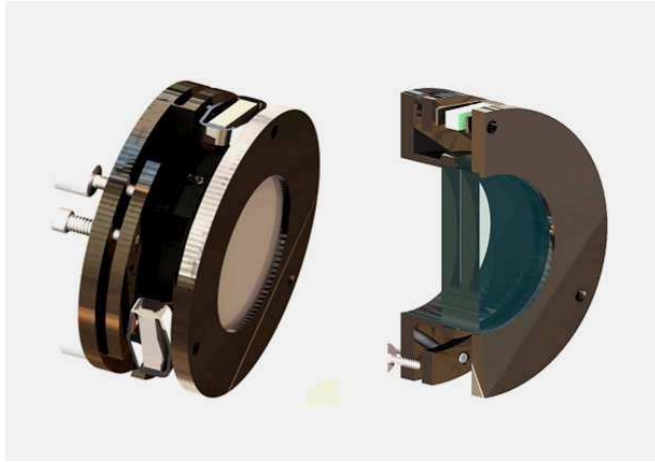

Fig. 15. Rendering of the F-P device and its section. The piezo actuator and the trimming screws are visible
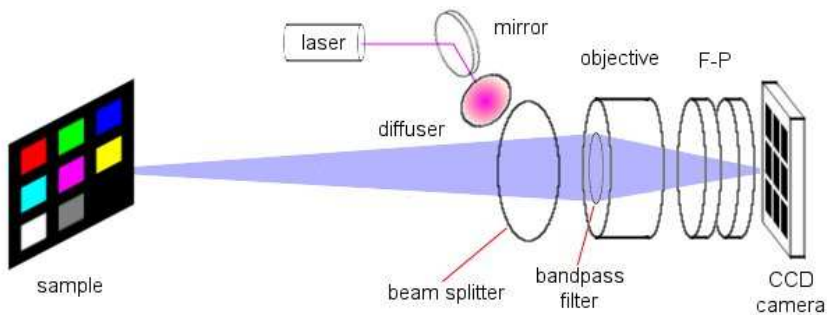

Fig. 16. Optical set-up formed by a beam splitter to couple the laser radiation to calibrate the retardation, the bandpass filter, the photographic objective and the CCD camera

The optical part of the HSIS is made of a photographic objective coupled with a CCD camera. The F-P is placed as close as possible to the camera sensor. Between the objective and the F-P is placed the optical band pass filter needed to select the wanted portion of the spectrum as explained before in order to apply the algorithm to find the missing points. The layout of the experiment used to obtain the data described in next section is schematized in

Fig 16. Other setups used in this work are variations of this one. The laser radiation to calibrate the mirror displacement is sent either directly on the sample or directly to the CCD through the F-P by inserting a beam splitter on the optical axis. We have used the HSIS in two different regions of the spectrum, in the visible by means of an optical band pass filter (380 – 720 nm), a reference blue laser at 410 nm and a 12-bit Si–CCD camera, in the NIR using a calibration laser at 980 nm and a 14-bit InGaAs CCD camera that has a response in the optical region 900 – 1700 nm.
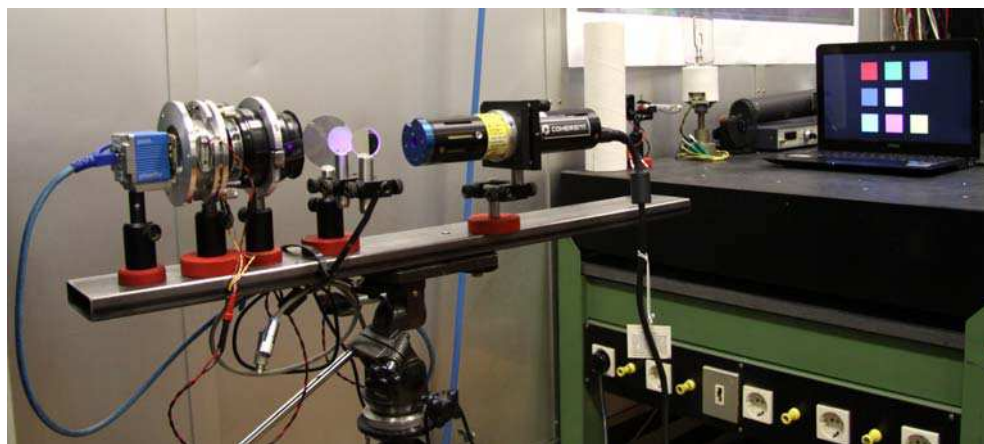

Fig. 17. Picture of the experiment where it has been acquired the spectrum of a laptop monitor

The HSIS is controlled by two boards on a PC, one used to drive the F-P and the other to drive the camera. The first, equipped with a 16-bit digital-to-analog converter, generates a triangular voltage ramp sent to a HV amplifier which generates the 0-100 V signal to drive the three piezo actuators (connected in parallel). Through the same board a trigger signal is generated synchronously with the ramp. The second board acquires a video starting from the trigger signal (corresponding to the maximum mirror distance condition) and ending with complete contact. In order to have a sufficient sampling rate to respect Nyquist criterion, about 1000 frames each acquisition are required for a 20 μm scan. This figure, in combination with the maximum frame rate of the camera sets the maximum ramp speed. The video is saved in TIFF format.

5. Hyperspectral imaging applications

This section shows some application of our HSIS prototype. We start with a calibrated reflective target to test the accuracy of the system, on a selectively absorptive target to test the potentialities as a spectroscopic analytic instrument, with laser sources to test the spectral resolution and on a heated tungsten plate to test thermal imaging.

5.1 Reflective target
The first application of the HSIS is a ColorChecker®. The image covers a rectangle of about 670x460 pixels on the CCD area. Each colour tab is illuminated by a laser spot in order to calibrate the retardation for each frame in the video. In Fig 18 a video frame is presented.
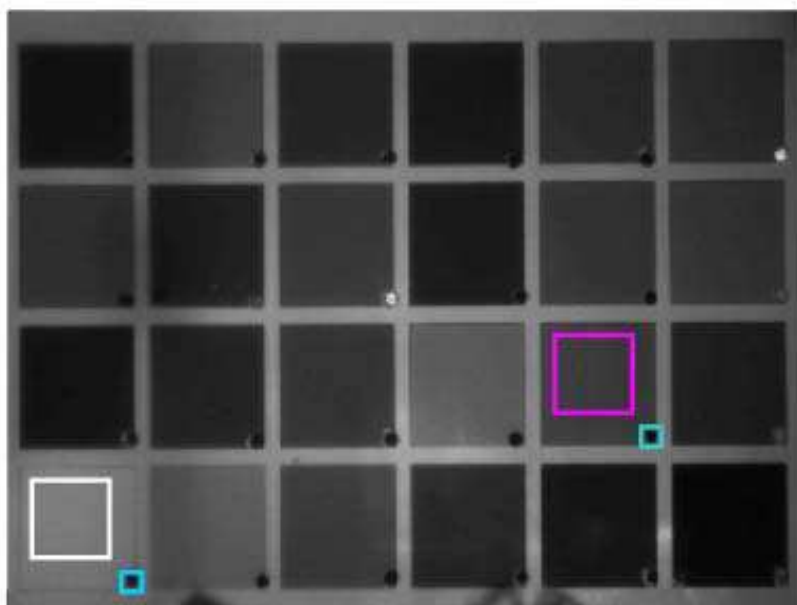
Fig. 18. Video frame of the colour checker target. In magenta and white are indicated the areas used for the calculation of the spectrum of the magenta and white tabs. In blue are indicated the pixels used to calibrate the retardation for both tabs
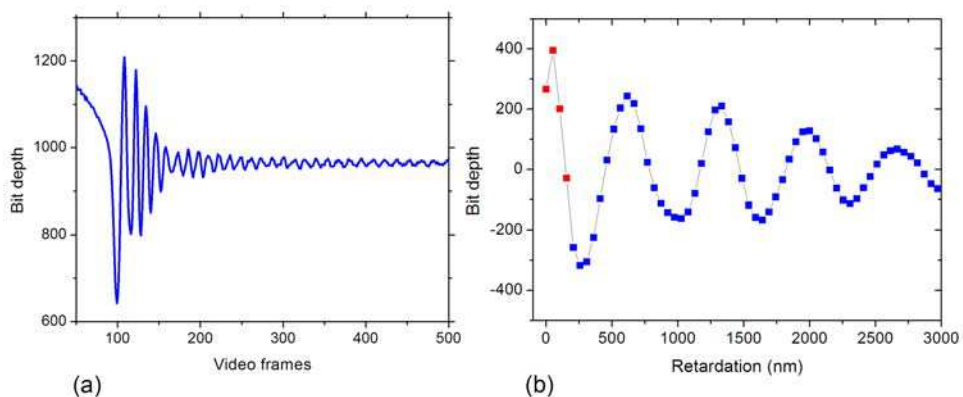

Fig. 19(a). the interferogram of the magenta set of pixels in Fig 18; Fig 19(b) the same interferogram after having subtracted the mean and calibrated the retardation using the calibration of the blue laser. The blue squares are the recorded data, the red squares are the values found with the reconstruction algorithm

The magenta square in Fig 18 contains the pixels used for the calculation of the spectrum of the magenta coloured tab. The blue square on the bottom right hand side contains the pixels

illuminated by the blue laser used to calibrate the retardation for the magenta. The same applies for the white tab (bottom left) used for normalization purposes. Fig 19(a) reports the interferogram of the pixel set in the magenta square in Fig 18 with the x-axis represented in video frames. In Fig 19(b) the blue squares are the first part of the same interferogram after the re-sampling using the reference scale from Fig 6(b) (as explained in section 4). The retardation sampling interval is 51.25 nm and the first record corresponds to a retardation of 205 nm (half wavelength of the blue laser).

The spectra obtained with the reconstructing algorithm are presented in Fig 20(b) (in black and magenta respectively the spectra of the white and magenta tabs). The resolution in frequency is about 14 THz corresponding to a resolution in wavelength of about 12 nm at a wavelength of 500 nm, (by applying the zero padding method the number of points is artificially increased in order to have one point each nanometer for practical computational reasons). The absolute reflectivity spectrum is given by the ratio of the coloured tab spectrum and the white tab spectrum used as a reference. In this way the effect of the non uniform spectral responses of the optical system, of the camera and of the light source is cancelled. In Fig 20(a) the reflectivity spectrum is shown and compared with the same spectrum measured with a commercial spectrometer (thin black line); relatively large differences are evident at the extremes of the spectrum mainly due to the reduced intensity of the reference spectrum in Fig 20(b).

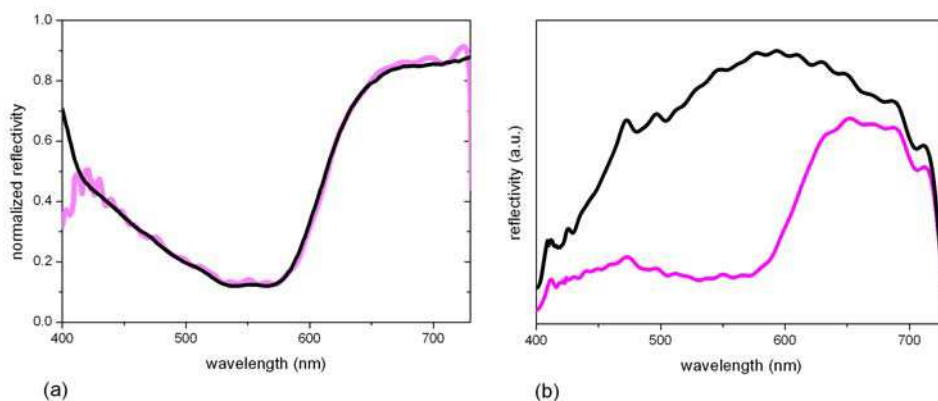(a)   (b)

Fig. 20. (a) Magenta spectrum normalized with respect to the white to obtain the absolute reflectivity spectrum, the black trace is the reflectivity spectrum obtained with a spectrometer. (b) In black and magenta respectively the spectra of the white and magenta tabs

Similarly we can obtain a hyperspectral image from an emitting surface. Fig 21 shows the emission spectra from a target made of LED and lamp sources. Even in this case a normalization that allows to take in account the responsivity of the whole system is necessary. The normalization in this case has been done comparing the spectrum obtained from a broadband source (a tungsten lamp or a white LED) with the same spectrum measured with a calibrated spectrophotometer. This normalization function is a constant of the system.
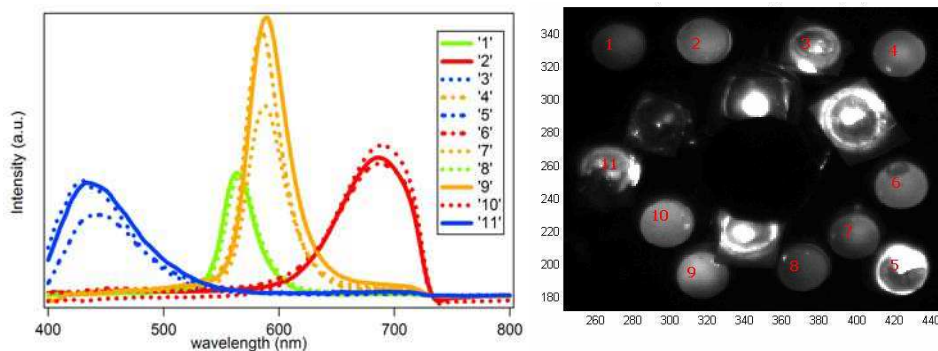
Fig. 21. The emission spectra on the left correspond to the pixel area (10×10) indicated in the image on the right. The target is composed of LED of four different colors (blue, green, yellow and red)

5.2 Spectroscopy applications

As a second application we have measured the transmission of a didymium oxide optical filter, and the results are presented in Fig 22. A white screen placed in front of the camera is illuminated with the xenon discharge lamp. A portion of the field of view of the camera is covered with the filter so that the light reflected by the screen passes through it before entering the objective. Another portion is illuminated with the blue laser again used for the retardation calibration. The transmittance spectrum is obtained by the ratio between the spectrum of the filtered portion and the spectrum of the white portion of the same image. Again the result is compared with the measurement done with a spectrometer (black line). This was done to demonstrate the potentialities of the instrument to detect complex absorption spectra, thus to be used in spectroscopy based chemical analysis.
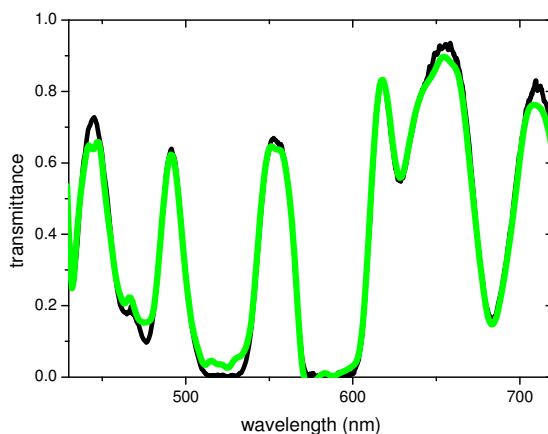

Fig. 22. The complex transmission spectrum of a glass doped with didymium oxide. The black line is the same spectrum measured with a classical spectrometer

5.3 Thermal imaging

The device can be used in different regions of the electromagnetic spectrum provided the transmissivity of the mirrors glass and the reflectivity of the metallic layer is adequate. We have implemented the system with a InGaAs camera capable of detecting infrared radiation in the 900-1700 nm band. One interesting application in this region is thermal imaging. By exploiting the change in shape of the blackbody radiation curve with temperature it is possible to infer the temperature of the emitting body. Fig 23 shows thermal imaging of a heated tungsten plate. With respect to classical thermal cameras which infer the temperature of a body by measuring the amount of radiation emitted in a given band, with an hyperspectral system the temperature is inferred by fitting the blackbody curve. The difference is that in the latter we do not need an *a priori* knowledge of the emissivity of the body.
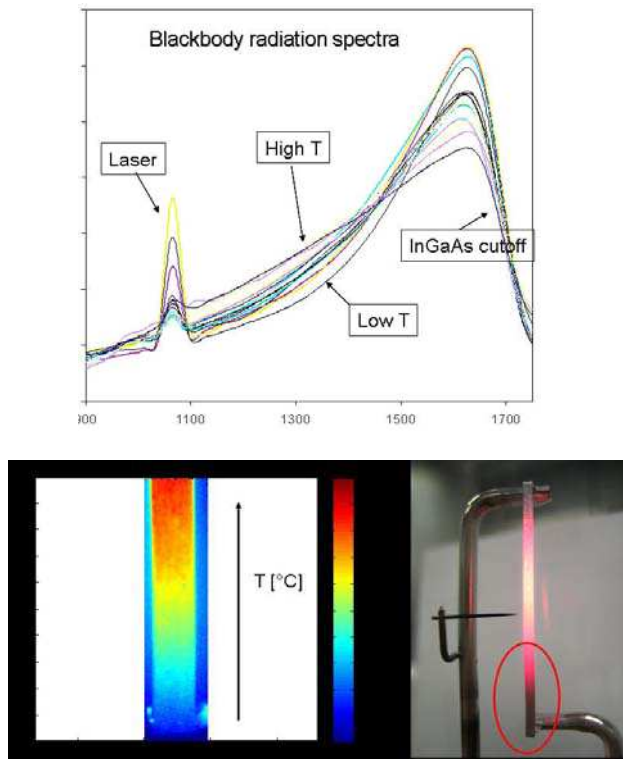

Fig. 23. Up: spectra obtained at different temperatures. The curves represent the blackbody emission spectra truncated by the responsivity of the camera for wavelengths larger than 1700 nm

5.4 Spectral resolution

In order to test the spectral resolution of the device a white target has been illuminated with lasers at five different wavelengths: a blue diode laser at 410 nm (used as a reference), a green duplicated Nd:YAG laser at 532.4 nm, a red He-Ne laser at 633 nm and two red diode lasers (637.5 and 674 nm). The scan applied to the mirrors is 50 μm corresponding to about

240 entire fringes in the blue interferogram. Fig 24 shows the obtained spectrum using Welch windowing. The experimental FWHM is about 3 THz corresponding to the theoretical resolution in eq. (8). The maximum difference of the measured wavelengths with respect to the nominal values is 1 nm. The resolution can be appreciated in the pair 633 and 638 nm whose peaks are well distinguishable.
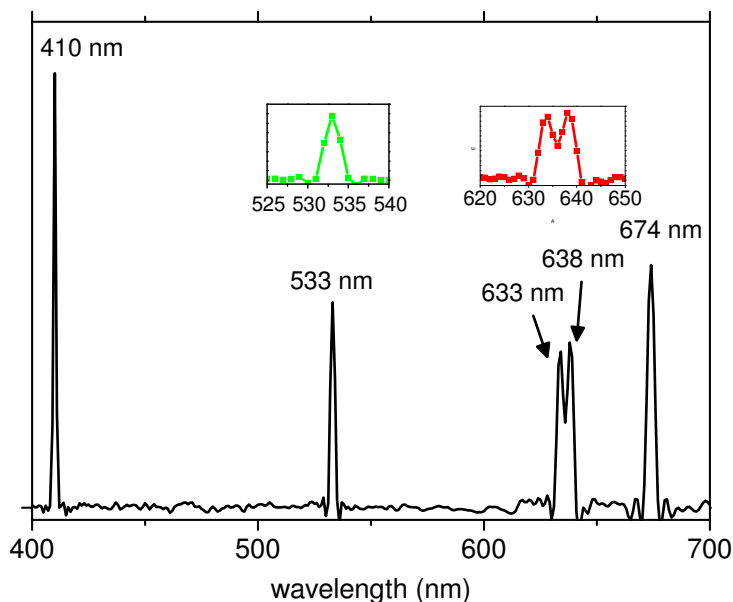

Fig. 24. Spectrum of a target illuminated by five laser beams having wavelength 410 nm (used as a reference), 532.4 nm, 633 nm, 637.5 nm and 674 nm. In the box a zoom of the green line showing the resolution

6. Conclusion

Hyperspectral imaging is a technique that consists in associating to each pixel of an image the spectral composition of the light hitting the same. The simplest example of Hyperspectral imaging is the RGB standard where color content of digital images is represented by giving the amount of red, green and blue. In a similar way we have three different cone cells in our retina, sensible to the three colors. By increasing the number of components of the spectral content would permit to have more information about the radiation emitted or reflect by an object. There are many applications to this technique in different fields, to mention but a few: fluorescence microscopy, thermal imaging, chemistry (infrared spectroscopic analysis), space missions (Earth survey for environmental or security), colorimetry. In this work we have realized a hyperspectral imaging device based on a Fabry-Perot interferometer. We have introduced the algorithm based on the Fourier transform to obtain the spectral content of each pixel from the measured interferogram. Moreover we have discussed the accuracy and resolution that characterize this system and some applications.

7. Acknowledgements

8. References

Alcock, R. D. & Coupland, J. M. (2006). A compact, high numerical aperture imaging Fourier transform spectrometer and its application. *Meas. Sci. Technol.,* Vol. 17, No. 11, (November 2006) page numbers (2861-2868), ISSN 0957-0233

Griffiths P. R. & de Haseth, J. A. (2007). *Fourier Transform Infrared Spectroscopy,* Wiley Interscience, ISBN 978-0-471-19404-0, Hoboken (U.S.A)

Pisani, M. & Zucco, M. (2009). Compact imaging spectrometer combining Fourier transform spectroscopy with a Fabry-Perot interferometer. *Optics Express,* Vol. 17, No. 7, (May 2009) page numbers (8319-8331), ISSN 1094-4087

Sellar, R. G. & Boreman, G. D. (2005). Classification of imaging spectrometers for remote sensing applications. *Opt Eng.,* Vol. 44, No. 1, (December 2004) page numbers (2861-2868), ISSN 0091-3286

Smith, S. W. (1999). *The Scientist and Engineer's Guide to Digital Signal Processing,* California Technical Publishing, ISBN 0-9660176-4-1, San Diego (U.S.A)

Weisstein, E. W. Apodization Function. From MathWorld--A Wolfram Web Resource. http://mathworld.wolfram.com/ApodizationFunction.html

Fourier Transforms - Approach to Scientific Principles

Edited by Prof. Goran Nikolic

This book aims to provide information about Fourier transform to those needing to use infrared spectroscopy, by explaining the fundamental aspects of the Fourier transform, and techniques for analyzing infrared data obtained for a wide number of materials. It summarizes the theory, instrumentation, methodology, techniques and application of FTIR spectroscopy, and improves the performance and quality of FTIR spectrophotometers.

How to reference

In order to correctly reference this scholarly work, feel free to copy and paste the following:

Marco Q. Pisani and Massimo E. Zucco (2011). Fourier Transform Based Hyperspectral Imaging, Fourier Transforms - Approach to Scientific Principles, Prof. Goran Nikolic (Ed.), ISBN: 978-953-307-231-9, InTech, Available from: http://www.intechopen.com/books/fourier-transforms-approach-to-scientific-principles/fourier-transform-based-hyperspectral-imaging

INTECH
open science | open minds